## PAPER

# Tailoring the phosphorus release from biochar-based fertilizers: role of magnesium or calcium addition during co-pyrolysis†

Kaewta Jetsrisuparb,[ab] Thanawan Jeejaila,[a] Chanon Saengthip,[a] Pornnapa Kasemsiri,[ab] Yuvarat Ngernyen,[a] Prinya Chindaprasirt[bc] and Jesper T. N. Knijnenburg [ID] *[bd]

The presence of magnesium (Mg) and calcium (Ca) in biochar-based fertilizers is linked to the slow release of phosphorus (P), but these alkali metals have not been systematically compared under identical conditions. In this study, sugarcane filter cake was treated with $H_3PO_4$ and MgO or CaO followed by pyrolysis at 600 °C to produce a Mg/P-rich biochar (MgPA-BC) and a Ca/P-rich biochar (CaPA-BC), respectively. The P-loaded biochars were studied by extraction and kinetic release in water over 240 hours to assess the potential P availability. X-ray diffraction and Fourier-transform infrared (FTIR) spectroscopy were used to characterize the pristine and post-kinetics biochars to identify the responsible phases for phosphate release. Additionally, the dissolved P concentrations in the kinetic release experiment were compared to thermodynamic solubility calculations of common Mg and Ca phosphates. Both MgPA-BC and CaPA-BC had P loadings of 73–74 g $kg^{-1}$ but showed distinctly different release behaviors. Phosphate dissolution from MgPA-BC was gradual and reached 10 g P per kg biochar after 240 hours, with rate-determining phases being $Mg_2P_2O_7$ (Mg pyrophosphate), $MgNH_4PO_4\cdot6H_2O$ (struvite), and $Mg_3(PO_4)_2\cdot22H_2O$ (cattiite). In contrast, CaPA-BC only released 1.2 g P per kg biochar. Phosphate release from CaPA-BC was limited by the low solubility of $Ca_2P_2O_7$ (Ca pyrophosphate) and $(Ca,Mg)_3(PO_4)_2$ (whitlockite). Co-pyrolysis with MgO retained P in a more soluble and available form than CaO, making MgO a preferential additive over CaO to immobilize phytoavailable P in biochar-based fertilizers with higher fertilizer effectiveness.

## 1. Introduction

Phosphorus (P) is an element that is indispensable for living organisms. Globally, many soils have low available P concentrations, and water-soluble P sources have been excessively applied to meet crop requirements. However, only a fraction of the applied P is taken up, and most of it is lost to surface waters through runoff or bound to soil in unavailable forms.[1] Ideally, the P release from fertilizers should be synchronized with crop demands in order to improve fertilizer use efficiency and minimize negative environmental impacts, which can be successfully realized in the form of slow release fertilizers.[2]

Thailand is the world's 4th largest producer of sugarcane with a production rate of over 100 million tons of sugarcane per year.[3] The main solid waste product in the sugar production process is sugarcane filter cake, a nutrient-rich residue that is left behind when cane juice is filtered. Each ton of crushed sugarcane produces 30–40 kg filter cake.[4] Due to its high nutrient content (1–2% of each nitrogen (N) and P per dry weight), the filter cake is often directly used as fertilizer,[4] but this may result in eutrophication due to losses of water-soluble nutrients like N and P to surface waters.[5]

Biochar is a porous carbon-rich material that is produced by thermal treatment of biomass in an oxygen-limited environment. Soil application of biochars can provide (long-term) financial gains to farmers,[6,7] and the conversion of sugarcane filter cake into a stable biochar presents an attractive solution to convert this waste into a valuable nutrient-rich soil amendment.[8–10] Compared to the raw biomass, biochars have a higher P content in a less water-soluble form with reduced leaching.[11,12] Especially the presence of calcium (Ca) and magnesium (Mg) aid to immobilize the P into forms that do not rapidly dissolve in water but are still available to crops.[13,14] The

*[a]Department of Chemical Engineering, Khon Kaen University, Khon Kaen 40002, Thailand*

*[b]Sustainable Infrastructure Research and Development Center, Khon Kaen University, Khon Kaen 40002, Thailand. E-mail: jespth@kku.ac.th*

*[c]Department of Civil Engineering, Khon Kaen University, Khon Kaen 40002, Thailand*

*[d]International College, Khon Kaen University, Khon Kaen 40002, Thailand*

conversion of a waste biomass such as sugarcane filter cake into a biochar may thus present an attractive slow release P fertilizer.

To further increase the P loading, biochars are frequently treated with a P source either before or after pyrolysis, and especially pre-pyrolysis treatment of the biomass with P in combination with Ca and/or Mg can produce slow release fertilizers.[15] Sugarcane leaves treated with MgO and a P source followed by pyrolysis at 600 °C produced biochar-based fertilizers that presented slow P release in water. Without MgO, the acidic P was rapidly released, highlighting the essential presence of Mg.[16] Similarly, the presence of Ca and Mg greatly reduced the water solubility of P when poultry litter was co-pyrolyzed with various P sources, with and without the addition of MgO.[17] Biochar-based fertilizers synthesized by co-pyrolysis of cotton straw with bentonite and $K_3PO_4$ under microwave irradiation had slow release of P and K in soil and were effective in increasing the growth of pepper seedlings in a pot trial.[18] Co-pyrolysis of sewage sludge (a P-rich waste) with CaO produced a biochar that could promote the growth of rice seedlings in hydroponic experiments.[19] Sewage sludge biochars modified with $MgCl_2$, CaO and MgO (but not $CaCl_2$) were effective at adsorbing P from solution. The Mg-modified biochars had a higher P release rate than the CaO-modified biochar. Adsorbed P was suggested to be rapidly released, whereas the inherent P in the biochars was released more slowly.[20] Also the co-pyrolysis of sawdust and switchgrass with triple superphosphate or bone meal at 500 °C produced P-loaded biochars with slow P release kinetics in water.[21]

In these previous studies, the gradual P release from biochar-based fertilizers has been linked to the presence of poorly soluble Mg and/or Ca phosphate phases. However, the differences in conditions used (e.g., pyrolysis temperature, raw material, and contents of Mg, Ca and P) make it difficult to directly compare the roles of Mg and Ca. Moreover, few studies have investigated the changes in the biochar during phosphate dissolution process,[17] and dissolved P concentrations have been rarely compared with thermodynamic solubility values of the phosphates.[22] In this work, sugarcane filter cake was pre-treated with $H_3PO_4$ and either MgO or CaO, and subsequently pyrolyzed at 600 °C. The P-loaded biochars were studied for their extractable P concentrations in 2% formic acid and deionized (DI) water, and the phosphate release kinetics were evaluated in DI water over 240 hours. To identify the phosphate release mechanism, the pristine and post-kinetics biochars were characterized by X-ray diffraction and FTIR spectroscopy. The proposed formation and dissolution mechanism of the formed Ca/Mg phosphate phases in the biochars supported by thermodynamic solubility calculations is presented.

# 2. Materials and methods

## 2.1 Materials

Dried sugarcane filter cake was obtained from Mitr Phol sugar factory (Chaiyaphum province, Thailand). The as-received filter cake was milled by ball mill to obtain a homogeneous powder. Phosphoric acid ($H_3PO_4$, ≥85%, RCI Labscan, Thailand), magnesium oxide (MgO, ≥97%, RCI Labscan, Thailand),

calcium oxide (CaO, ≥90%, Kemaus, Australia), formic acid (99%, APS Chemicals, New Zealand), and ammonium persulfate (98%, Loba Chemie, India) were used as received. All solutions were prepared with DI water (18.2 MΩ).

## 2.2 Preparation of biochars

To prepare the modified biochars, the dry filter cake powder was first manually mixed with a given amount of MgO or CaO until a homogeneous mixture was obtained. Each solid mixture was then immersed in a solution of 1 M $H_3PO_4$. Caution was taken when adding the $H_3PO_4$ solution because the reaction of $H_3PO_4$ with MgO and especially with CaO was highly exothermic.[23] The pre-treatment with $H_3PO_4$ in combination with MgO or CaO was carried out at a P : biomass ratio of 1 : 12 (w/w) and the atomic ratios of respectively P : Mg or P : Ca were 1 : 1.[16,17] After drying, the pre-treated biomasses (200–300 g per batch) were packed into enclosed clay pots and pyrolysis was done in a muffle furnace at 600 °C for 3 h (heating rate of 6 °C min$^{-1}$) based on our previous study.[16] The biochar yield was calculated by dividing the mass of the produced biochar by the mass of the treated filter cake prior to pyrolysis. An unmodified biochar was prepared under the same pyrolysis conditions.

Three biochars were produced: (i) unmodified filter cake biochar (BC), (ii) filter cake biochar pre-treated with $H_3PO_4$ and MgO (MgPA-BC), and (iii) filter cake biochar pre-treated with $H_3PO_4$ and CaO (CaPA-BC).

## 2.3 Characterization of biochars

The ash contents of the biochar were determined in triplicate by ashing 0.2 g biochar at 500 °C for 8 h. Nitrogen adsorption experiments were carried out at 77 K on a Micromeritics ASAP 2460 (Micromeritics, USA) by measuring a 41-point adsorption–desorption isotherm for each sample. The samples were degassed overnight under vacuum at 200 °C prior to analysis. The BET specific surface area ($S_{BET}$) was determined at a relative pressure ($P/P^0$) range of 0.05–0.25, the total pore volume ($V_T$) was determined at $P/P^0 \geq 0.95$, the micropore volume ($V_{micro}$) was obtained from the t-plot, and the average pore diameter ($D_p$) was calculated with the BJH method using desorption data.

X-ray diffraction (XRD) measurements were carried out on a PANalytical EMPYREAN diffractometer (PANalytical B.V., the Netherlands) with Cu Kα radiation operating at 40 kV and 45 mA. Patterns were collected over $2\theta = 5$–70° with step size 0.02 s$^{-1}$. The crystalline phases were identified using X'Pert High-Score Plus software (PANalytical B.V., the Netherlands). Fourier transform infrared (FTIR) spectra were collected on a Bruker Alpha II ATR-FTIR (Bruker, Germany) at 4000–600 cm$^{-1}$ (32 scans, resolution 2 cm$^{-1}$). Scanning electron microscopy (SEM) analysis was done on a Hitachi SU3800 (Hitachi, Japan) after sputter-coating the samples with gold.

The total metal (Ca, Mg, Fe, and K) and P contents of the biochars were determined in triplicate after digesting the biochars by modified dry ashing.[24] After filtration, the Ca, Mg, Fe, and K concentrations were measured by flame atomic absorption spectroscopy on a PinAAcle 900F (Perkin Elmer, Singapore) after dilution in 1% $HNO_3$. For Ca and Mg measurements, each

standard and sample solution contained 1000 ppm Sr to eliminate interferences. The P concentrations were measured by UV-vis spectroscopy (Agilent 8453, Agilent Technologies, USA) *via* the molybdenum blue method at 880 nm.[25]

The extractable P of the biochars was evaluated in DI water and 2% formic acid according to the modified method of Wang *et al.*[26] The suspensions (0.3 g biochar in 30 mL extractant) were ultrasonicated for 10 min and placed on an orbital shaker (Gallenkamp, UK) at 120 rpm. After 30 min, the suspensions were filtered through a 0.22 μm nylon filter and the extracted P concentrations were measured by UV-vis spectroscopy *via* the molybdenum blue method. The pH values of the extracts in DI water were recorded with a digital pH meter (OHAUS Starter 3100, OHAUS Corporation, USA), and the average value for each sample was reported as the biochar pH.[16]

### 2.4 Phosphorus release from biochar-based fertilizers

The slow release behavior of phosphate from MgPA-BC and CaPA-BC was studied in triplicate.[16,27] The suspensions (1.0 g biochar in 200 mL DI water) were gently mixed (100 rpm) on an orbital shaker (Gallenkamp, UK) in a closed Erlenmeyer flask for 240 hours at room temperature. Periodically, a 2 mL sample was filtered (nylon filter, 0.22 μm) and the dissolved phosphate concentrations were determined with UV-vis spectroscopy *via* the molybdenum blue method. The solution pH was measured at each collection point after sample withdrawal.

The following models were used to describe the phosphate dissolution kinetics: zero order, pseudo-first order, pseudo-second order, Elovich, parabolic diffusion, and power function (Table S1 in ESI†). The suitability of each model to describe the release behavior was assessed by the coefficient of determination ($R^2$) and the standard error of the estimate (SE).[16]

At the end of the kinetic release experiment (after 240 hours) the biochars were collected by filtration (Whatman no. 42, GE Healthcare Life Sciences, UK), rinsed with DI water, dried for 24 hours at 40 °C, and subsequently analyzed by XRD and FTIR spectroscopy as described previously. These post-kinetics biochars are referred to as MgPA-BC-post and CaPA-BC-post. The Ca and Mg contents in the filtrate after 240 hours were measured by AAS as described previously. Additionally, the solution after 240 hours was digested with ammonium persulfate according to the procedure of Huang and Zhang[28] with slight modifications. Each solution was mixed with 6 mL DI water and 1.2 mL of a 4.2% ammonium persulfate solution in a 10 mL screw-cap vial. The vials were tightly closed and

digestion was carried out in an oven (Biobase BOV-V45F, Biobase Bioindustry Co. Ltd, China) for 16 hours at 90 °C. The P concentration of each sample after persulfate digestion was determined by UV-vis spectroscopy *via* the molybdenum blue method.

### 2.5 Thermodynamic solubility calculations

The solubility of various Mg and Ca phosphates as function of pH was calculated with ChemEQL software (version 3.2)[29] assuming ideal conditions. The solubility products of the used phases are given in Table S2 (ESI).†

## 3. Results and discussion

### 3.1 General properties of the biochars

Selected properties of the produced sugarcane filter cake biochars are summarized in Table 1. The yield of the unmodified sugarcane filter cake biochar (BC) was 64.3%, which is higher than other biochars produced under comparable conditions.[30] The high yield may be due to the high ash content (77.5%) that indicated a substantial content of inorganic material. Previous studies on sugarcane filter cake biochars reported a yield of 42–68% and ash contents of 52–58% but at lower pyrolysis temperatures (350–380 °C).[10,31] Modification of the biochar with MgO and $H_3PO_4$ decreased the yield to 59.9% for MgPA-BC, as also observed previously for sugarcane leaf biochar.[16] In contrast, modification with CaO and $H_3PO_4$ increased the yield of CaPA-BC to 68.4%, which may be due to the higher atomic mass of Ca compared to Mg. The ash contents in MgPA-BC and CaPA-BC increased to 80.9–82.6% due to the introduction of Mg/Ca and P into the powders. The pH of the biochars ranged from 7.0 to 8.1, in agreement with previous studies.[10,32] Compared to BC, the lower pH of MgPA-BC and CaPA-BC may have been due to the presence of free acid groups from the pretreatment of the filter cake with $H_3PO_4$.

Sample BC contained small amounts of Ca (15.8 g kg$^{-1}$), Fe (10.9 g kg$^{-1}$), K (3.1 g kg$^{-1}$), and Mg (2.6 g kg$^{-1}$), which were similar to previous studies on sugarcane filter cake biochars.[10,32] In the treated biochars, the concentrations of Fe and K decreased to 6.0–6.9 g kg$^{-1}$ and 2.0–2.3 g kg$^{-1}$, respectively, likely due to leaching during pretreatment and dilution due to additive addition. As expected, the Mg content in MgPA-BC increased greatly to 40.9 g kg$^{-1}$. This Mg content was higher than that of sugarcane leaf biochars[16] modified with Mg and P but lower than other Mg-modified biochars.[17] The Ca content in MgPA-BC conversely decreased to 0.9 g kg$^{-1}$, which could have

**Table 1** General properties and composition of the sugarcane filter cake biochars. Ash and elemental contents are given as mean ($n = 3$) ± standard deviation

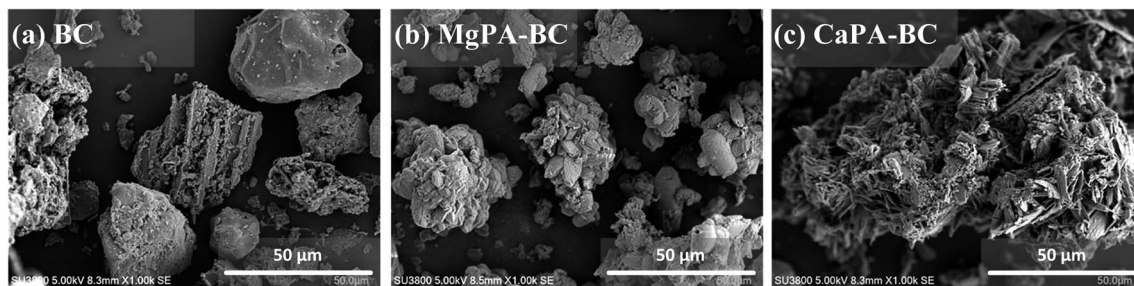| Sample | Yield (%) | pH | Ash (wt%) | Ca (g kg$^{-1}$) | Mg (g kg$^{-1}$) | Fe (g kg$^{-1}$) | K (g kg$^{-1}$) | P (g kg$^{-1}$) | P : Mg | P : Ca |
|---|---|---|---|---|---|---|---|---|---|---|
| BC | 64.3 | 8.1 | 77.5 ± 2.6 | 15.8 ± 1.2 | 2.6 ± 0.2 | 10.9 ± 1.1 | 3.1 ± 0.3 | 12.0 ± 1.1 | 3.7 | 1.0 |
| MgPA-BC | 59.9 | 7.7 | 80.9 ± 0.9 | 0.9 ± 0.1 | 40.9 ± 2.7 | 6.0 ± 0.8 | 2.0 ± 0.2 | 74.1 ± 7.3 | 1.4 | 110.5 |
| CaPA-BC | 68.4 | 7.0 | 82.6 ± 1.1 | 92.1 ± 4.6 | 2.4 ± 0.1 | 6.9 ± 0.7 | 2.3 ± 0.4 | 73.4 ± 2.6 | 24.2 | 1.0 |

Fig. 1 Scanning electron microscopy (SEM) images of (a) BC, (b) MgPA-BC, and (c) CaPA-BC at 1000× magnification.

been caused by the leaching of Ca in the $H_3PO_4$ pre-treatment solution. Upon pre-treatment with CaO and $H_3PO_4$, the Ca content in CaPA-BC greatly increased to 92.1 g $kg^{-1}$, similar to previous works.[17,19]

The P content of BC was 12.0 g $kg^{-1}$ which is typical for sugarcane filter cake biochars,[10,32] and increased to 73.4–74.1 g $kg^{-1}$ for the modified biochars. Such P loadings are comparable to previous works.[16,17,21,33] The modified biochars had an approximately equimolar ratio of P to additive cation: the P : Mg ratio in MgPA-BC was 1.4, and the P : Ca ratio in CaPA-BC was 1.0.

Biochar morphology was studied by scanning electron microscopy (Fig. 1). The unmodified filter cake biochar (BC) was heterogeneous with particles originating from plant fibers in the sugarcane and angular particles that were likely inorganic compounds.[5] Compared to BC, the particle size of MgPA-BC was smaller which may have been a result of the pre-treatment with $H_3PO_4$. The MgPA-BC consisted of agglomerates of crystalline particles, which were likely a Mg phosphate such as $Mg_2P_2O_7$.[16] In contrast to MgPA-BC, CaPA-BC was more agglomerated and showed the presence of needle-like or tabular particles, possibly $Ca_2P_2O_7$.[34]

### 3.2 Specific surface area and porosity

The unmodified sugarcane filter cake biochar (BC) had a specific surface area ($S_{BET}$) of 32.9 $m^2$ $g^{-1}$ (Table 2). This $S_{BET}$ was lower than plant-derived biochars produced under similar conditions but comparable to biochars derived from biosolids[30] and sugarcane filter cake biochars produced under similar conditions.[8,9] Both pre-treatments slightly increased the $S_{BET}$ and $V_T$, and slightly decreased the average pore diameter ($D_p$), suggesting a small promoting effect of the additives on biochar

pore formation. The $N_2$ adsorption experiment demonstrated that the pores consisted of only 14–18% of micropores. Generally, biochars with high ash contents (as is the case here) have low porosity because pore development largely depends on the release of volatile matter during pyrolysis.[35]

### 3.3 Extractable P

The slow P release potential of the biochars was assessed by measuring the extractable P in 2% formic acid (FA) and DI water (DIW) (Fig. 2). Here, FA was used as extraction solution because it provides a good indication of P phytoavailability from high-ash biochars.[26] All biochars contained a very small amount of DIW-extractable P (<1 g $kg^{-1}$) that accounted for only 1–2% of the total P present in those materials, comparable to previous studies.[12,19] Since the P release from such biochars is proton-promoted, the alkaline nature of the biochars (pH 7.0–8.1, Table 1) likely limited the P release in water.[12] In BC, the FA-extractable P was 8.4 g $kg^{-1}$, which accounted for 70% of the total P (12 g $kg^{-1}$, Table 1), indicating that the majority of the P in BC was available to crops. The total P loading, however, was low.

Table 2 BET specific surface area ($S_{BET}$), micropore volume ($V_{micro}$), total pore volume ($V_T$), and average pore diameter ($D_p$) of the different biochars. Percentages in brackets represent the contribution of $V_{micro}$ to $V_T$

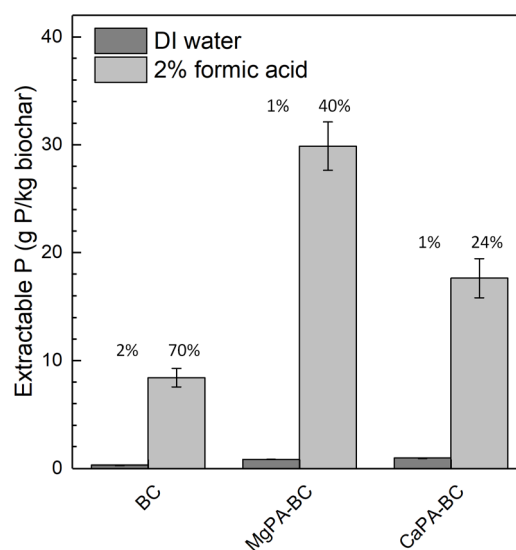| Material | $S_{BET}$ ($m^2$ $g^{-1}$) | $V_{micro}$ ($cm^3$ $g^{-1}$) | $V_T$ ($cm^3$ $g^{-1}$) | $D_p$ (nm) |
|---|---|---|---|---|
| BC | 32.9 | 0.010 (18%) | 0.054 | 11.7 |
| MgPA-BC | 43.6 | 0.011 (14%) | 0.079 | 7.8 |
| CaPA-BC | 42.6 | 0.011 (16%) | 0.071 | 9.9 |



Fig. 2 Extractable P from the biochars in DI water (DIW) and 2% formic acid (FA). The values above the bars indicate the percentage of the total P that is extracted with each extraction solution.

Modification of the biochars greatly increased the FA-extractable P, ranging from 18 g kg$^{-1}$ (CaPA-BC) to 30 g kg$^{-1}$ (MgPA-BC). These values accounted for 24–40% of the total P in those materials, in agreement with previous studies.[16,26] Compared to Ca, particularly the modification with Mg-containing pre-treatments enhanced the P extractability; the percentage of total P in MgPA-BC that was FA-extractable (40%) was almost twice as large as that of CaPA-BC (24%). This may suggest that the P in MgPA-BC is more available to crops than that in CaPA-BC.

All biochars had a much higher FA-extractable P compared to the DIW-extractable P, which indicated the potential for slow release. Based on these results, both MgPA-BC and CaPA-BC were considered promising materials for slow P release fertilizers and were subsequently tested in a 240 hour release study in water.

### 3.4 Phosphate slow release behavior

The slow release behavior of MgPA-BC and CaPA-BC was evaluated in DI water over 240 hours. The phosphate release (Fig. 3a) and pH of the solutions at each time point (Fig. 3b) showed clear differences between the two materials. The phosphate release from MgPA-BC was initially small (only 1 g P per kg biochar after 1 hour), but this gradually increased to 4 g kg$^{-1}$ after 24 hours, and to 10 g kg$^{-1}$ after 240 hours. During dissolution, the pH was slightly alkaline and reached a value of 8.4 after 240 hours. In contrast, the phosphate release from CaPA-BC was much smaller; after 24 hours, only 0.9 g kg$^{-1}$ P was released, which only slightly increased to 1.2 g kg$^{-1}$ for 144 hours and then remained constant. The pH of the solution was lower as well and stabilized around 7.4. The higher phosphate release from MgPA-BC compared to CaPA-BC was in agreement with Fang et al.[20]

Six models were used to assess the phosphate release from the modified biochars (Table S1 in ESI†). Based on the $R^2$ and SE

**Table 3** Coefficients of determination ($R^2$) and standard error of the estimate (SE) of the kinetic models for phosphate release from biochars

| Model | MgPA-BC $R^2$/SE | CaPA-BC $R^2$/SE |
|---|---|---|
| Zero order | 0.87/1.46 | 0.67/0.23 |
| Pseudo-first order | 0.97/0.55 | 0.75/0.19 |
| Pseudo-second order | 0.97/0.97 | 0.99/0.19 |
| Elovich | 0.90/1.25 | 0.97/0.07 |
| Parabolic diffusion | 0.98/0.55 | 0.87/0.15 |
| Power function | 1.00/0.43 | 0.99/0.08 |

values, the phosphate release from both MgPA-BC and CaPA-BC was best described by the power function (Table 3). In previous studies, phosphate release from other biochars also followed the power function,[21,22] but also parabolic diffusion,[16,21] Elovich,[17] and even zero order equation[12] have been used. The constants for the power function were $a = 1.065$ g kg$^{-1}$ h$^{-0.42}$ and $b = 0.42$ (MgPA-BC), and $a = 0.478$ g kg$^{-1}$ h$^{-0.20}$ and $b = 0.20$ (CaPA-BC). For both biochars, the values of $b$ were less than 1, implying that the release rates decreased with time. For MgPA-BC, $b$ was close to 0.5, in which case the power function approaches the parabolic diffusion model; indeed, the parabolic diffusion model provided the second best fit (Table 3). The $a$ value represents the initial release rate, which indicated that MgPA-BC had an initial phosphate release rate that was more than twice as large as that of CaPA-BC. To identify the dissolution mechanism, the biochars were characterized by X-ray diffraction and FTIR spectroscopy before and after the kinetics dissolution experiments, and the results are presented in the next sections.
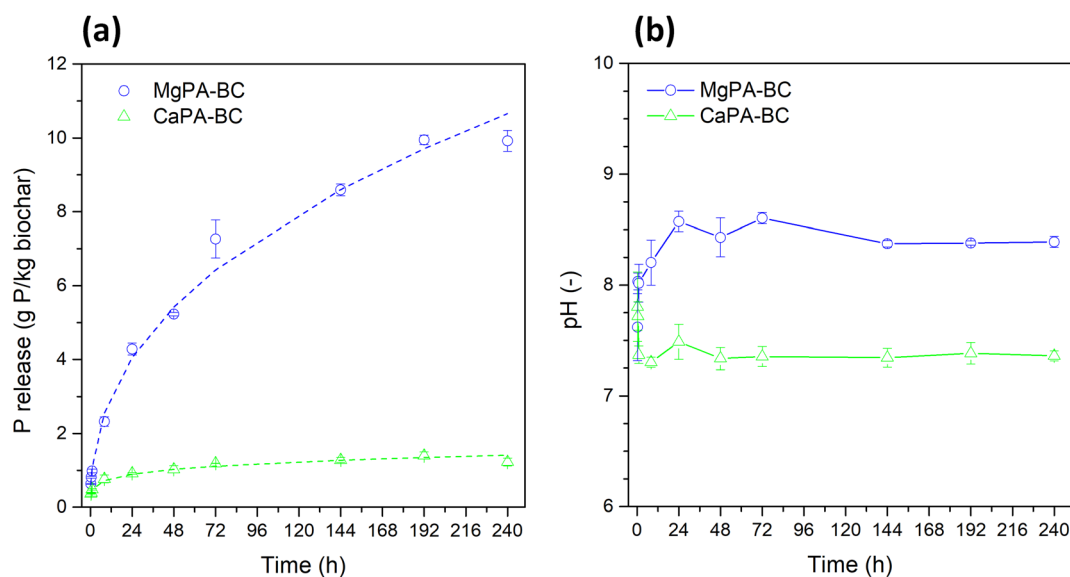


**Fig. 3** (a) Phosphate release and (b) pH of the corresponding solutions of the kinetic release experiment of MgPA–BC and CaPA–BC in DI water over 240 hours. Lines in (a) indicate the power function models that provided the best fit of the phosphate release kinetics.
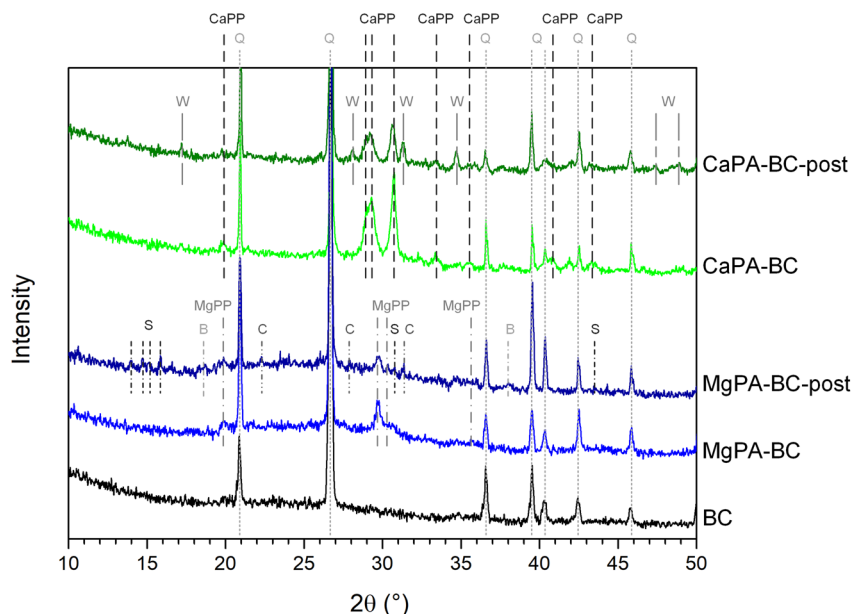
Fig. 4 X-ray diffraction patterns of pristine BC and MgPA-BC and CaPA-BC, and the modified biochars after the 240 hour kinetic release experiment (MgPA-BC-post and CaPA-BC-post, respectively). Abbreviations of the identified phases are as follows (corresponding JCPDS no. are given in brackets): Q, quartz ($SiO_2$, 78-2315); MgPP, magnesium pyrophosphate ($\alpha$-$Mg_2P_2O_7$, 32-0626); S, struvite ($MgNH_4PO_4 \cdot 6H_2O$, 15-0762) or struvite-K ($MgKPO_4 \cdot 6H_2O$, 35-0812); B, brucite ($Mg(OH)_2$, 07-0239); C, cattiite ($Mg_3(PO_4)_2 \cdot 22H_2O$, 35-0186); CaPP, calcium pyrophosphate ($Ca_2P_2O_7$, 17-0499); W, whitlockite (($Ca,Mg)_3(PO_4)_2$, 13-0404).

### 3.5 X-ray diffraction patterns of pristine and post-kinetics biochars

Fig. 4 shows the XRD patterns of the modified biochars before and after the kinetic release experiment. The pattern of the unmodified biochar (BC) displayed strong peaks at $2\theta = 20.9°$, $26.6°$, $36.5°$, $39.5°$, $40.3°$, $42.4°$, and $45.8°$ that were ascribed to quartz ($SiO_2$). No other crystalline phases were found in BC. In addition to quartz, the Mg-containing pre-treated biochar (MgPA-BC) presented peaks of crystalline Mg pyrophosphate (MgPP, $\alpha$-$Mg_2P_2O_7$), in agreement with previous studies.[16,17] After the kinetic study, the $Mg_2P_2O_7$ peaks in MgPA-BC-post have reduced in intensity, suggesting their dissolution or transformation. New peaks in MgPA-BC-post at $2\theta = 13–16°$ and $30.6°$ indicated the presence of small amounts of struvite ($MgNH_4PO_4 \cdot 6H_2O$) or struvite-K ($MgKPO_4 \cdot 6H_2O$), and peaks at $2\theta = 18.6°$ and $38.0°$ were ascribed to brucite ($Mg(OH)_2$). Small peaks at $2\theta = 22.3°$, $27.9°$, and $31.2°$ indicated that cattiite ($Mg_3(PO_4)_2 \cdot 22H_2O$) was present after the kinetic experiment in MgPA-BC-post.

The pristine Ca-containing pre-treated biochar (CaPA-BC) contained crystalline Ca pyrophosphate ($\gamma$-$Ca_2P_2O_7$), as also seen in previous studies where P-loaded biochars were formed by pre-treatment with Ca and P.[17,21,33] After the kinetic study, peaks for $Ca_2P_2O_7$ were still present in CaPA-BC-post but reduced in intensity, and new peaks corresponding to $(Ca,Mg)_3(PO_4)_2$, a Mg-stabilized $\beta$-$Ca_3(PO_4)_2$ phase sometimes referred to as whitlockite, were found at $2\theta = 17.0°$, $28.2°$, $31.5°$, $34.9°$, $47.4°$ and $48.9°$.

### 3.6 FTIR spectroscopy of pristine and post-kinetics biochars

Fig. 5 presents the FTIR spectra at 1800–600 $cm^{-1}$ of the pristine biochars and after the kinetic release experiment. Most

vibrations for phosphate groups appear in this region,[36,37] and no apparent peaks were observed at higher wavenumbers (Fig. S1 in ESI†). In the FTIR spectrum of BC, the peaks at 690, 777, 797, 1040–1100, and 1168 $cm^{-1}$ were ascribed to various Si–O vibrations in quartz.[38] The peaks at 1040–1100 $cm^{-1}$ may possibly indicate the presence of C–O stretching of alcohol and ether groups.[39] Peaks at 655 and 741 $cm^{-1}$ were ascribed to Si–O
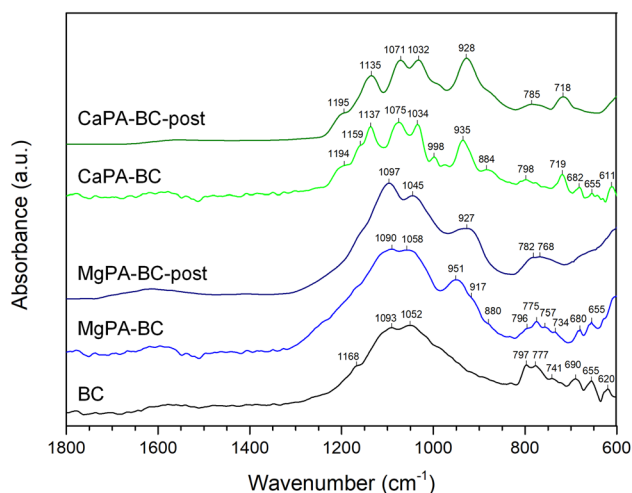


Fig. 5 FTIR spectra (1800–600 $cm^{-1}$) of pristine BC and MgPA-BC and CaPA-BC, and the modified biochars after the 240 hour kinetic release experiment (MgPA-BC-post and CaPA-BC-post, respectively). Approximate peak positions are indicated above each peak. The FTIR spectra over the full range (4000–600 $cm^{-1}$) can be found as Fig. S1 in the ESI.†

or Al–O vibrations in silicate minerals,[38] and the peak at 620 cm$^{-1}$ may be due to C–C stretching vibrations.[39]
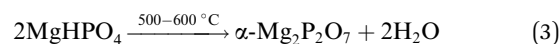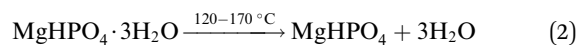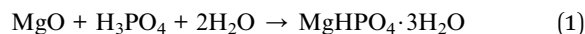
Upon pre-treatment with MgO and H$_3$PO$_4$, the FTIR spectrum of MgPA-BC showed a relative increase in peak intensity around 1090 cm$^{-1}$ compared to BC, possibly because of incorporation of a (pyro)phosphate,[36,40] likely Mg$_2$P$_2$O$_7$ as observed in the XRD patterns (Fig. 4). Possibly, the shoulder peak at 917 cm$^{-1}$ can also be ascribed to Mg$_2$P$_2$O$_7$.[41] The increased intensity of a peak around 951 cm$^{-1}$ indicated the presence of symmetric stretching mode of P–O bonds of orthophosphate groups,[42] and the shoulder at 880 cm$^{-1}$ was ascribed to HPO$_4$ group vibrations.[43] However, more information about the presence of specific phosphate phases in MgPA-BC was difficult to obtain due to the overlap of the phosphate vibrations with the Si–O peaks in the region 800–1300 cm$^{-1}$.

After the kinetic experiment, the peaks at 1045, 951, and 880 cm$^{-1}$ decreased in intensity, possibly suggesting the dissolution of an orthophosphate phase. As a result, the broader underlying peak with maximum at 927 cm$^{-1}$ was found in MgPA-BC-post (this peak was present in MgPA-BC but masked by the peak at 951 cm$^{-1}$ and only found as a shoulder at 917 cm$^{-1}$), which was ascribed to Mg$_2$P$_2$O$_7$.[41] At lower wavenumbers (600–800 cm$^{-1}$) peaks have become broader, possibly due to the formation of struvite[36] that has an absorbance peak at 770 cm$^{-1}$ that overlapped with the vibrational peaks of quartz. The cattiite (Mg$_3$(PO$_4$)$_2$·22H$_2$O) that was identified by XRD has its main absorbance peak[43] at 980 cm$^{-1}$ but this peak could not be confirmed with FTIR spectroscopy due to the low quantity and overlap with other quartz/phosphate peaks.

In the FTIR spectrum of CaPA-BC, the peaks at 611, 719, 935, 998, 1034, 1075, 1137, 1159, and 1194 cm$^{-1}$ were assigned to γ-Ca$_2$P$_2$O$_7$.[44] The peak at 884 cm$^{-1}$ indicated the presence of HPO$_4$ groups from amorphous CaHPO$_4$.[45] After the kinetic experiment, there was only little change in the FTIR spectrum of CaPA-BC-post compared to CaPA-BC. Various peaks have broadened, which may suggest a reduction in crystallinity and potentially a transformation of phosphate phases. Moreover, the HPO$_4$ peak at 884 cm$^{-1}$ reduced in intensity and broadened to become a shoulder peak, possibly indicating its dissolution. The (Ca,Mg)$_3$(PO$_4$)$_2$ as identified in the XRD pattern (Fig. 4) has its main FTIR absorbance peaks in the region 970–1120 cm$^{-1}$,[46] but the presence of these peaks could not be confirmed in CaPA-BC-post due to the overlap with the Ca$_2$P$_2$O$_7$ and SiO$_2$ vibrations.

### 3.7 Formation and dissolution mechanism of MgPA-BC

Based on the X-ray diffraction analysis (Fig. 4), MgPA-BC contained crystalline P in the form of α-Mg$_2$P$_2$O$_7$. This was further confirmed by the characteristic peaks of α-Mg$_2$P$_2$O$_7$ in the FTIR spectrum of pristine MgPA-BC (Fig. 5) and the presence of microsized crystals in the SEM image (Fig. 1b). In previous studies, Mg$_2$P$_2$O$_7$ was formed under similar pyrolysis conditions.[16,17] The formation of crystalline α-Mg$_2$P$_2$O$_7$ during biochar synthesis is proposed to occur according to the following reactions:

$$MgO + H_3PO_4 + 2H_2O \rightarrow MgHPO_4 \cdot 3H_2O \qquad (1)$$

$$MgHPO_4 \cdot 3H_2O \xrightarrow{120-170\,°C} MgHPO_4 + 3H_2O \qquad (2)$$

$$2MgHPO_4 \xrightarrow{500-600\,°C} \alpha\text{-}Mg_2P_2O_7 + 2H_2O \qquad (3)$$

Before pyrolysis, the reaction between MgO and H$_3$PO$_4$ in the pre-treatment process resulted in the formation of MgHPO$_4$·3H$_2$O.[47] Upon thermal treatment, dehydration of MgHPO$_4$·3H$_2$O took place around 120–170 °C and resulted in an amorphous MgHPO$_4$ phase.[48,49] Further heating converted this amorphous phase into crystalline α-Mg$_2$P$_2$O$_7$ that is formed around 500–600 °C depending on the particle size and heating conditions.[49,50] The conversion of amorphous MgHPO$_4$ into crystalline α-Mg$_2$P$_2$O$_7$ follows a complicated mechanism of various polyphosphate chain lengthening and shortening steps.[50]

However, Mg$_2$P$_2$O$_7$ was likely not the only P form in MgPA-BC. Aramendía et al.[51] estimated with solid-state $^{31}$P MAS NMR measurements that when MgHPO$_4$·3H$_2$O was heated to 650 °C the material consisted of a mixture of 15% crystalline Mg$_3$(PO$_4$)$_2$ and 85% crystalline α-Mg$_2$P$_2$O$_7$. At a lower temperature of 500 °C, the Mg$_3$(PO$_4$)$_2$ was amorphous and its proportion was larger than at 650 °C (i.e., >15%). These data suggested that MgPA-BC, which was produced at 600 °C, likely contained a substantial fraction of amorphous Mg$_3$(PO$_4$)$_2$ in addition to the crystalline α-Mg$_2$P$_2$O$_7$. This was also inferred from the presence of an orthophosphate peak at 951 cm$^{-1}$ in the FTIR spectrum of MgPA-BC (Fig. 5). In addition, other (amorphous) orthophosphate phases may have been present as well. Possibly, some struvite (MgNH$_4$PO$_4$·6H$_2$O) and/or struvite-K (MgKPO$_4$·6H$_2$O) may have been formed by the presence of respectively NH$_4^+$ and/or K$^+$ in the biomass.[47] Even though struvite is unstable at high temperatures (the loss of water and NH$_3$ from struvite takes place[41] below 300 °C), Bekiaris et al.[36] found indications that an amorphous struvite phase was present in biochar produced from a solid fraction of digestate at 600 °C. The presence of struvite in biochars was also suggested by Bruun et al.[11] from the co-occurrence of Mg and P in SEM-EDX analysis with high spatial correlation, and also Wang et al.[12] suggested that a Mg phosphate mineral (possibly struvite) was the main phase responsible for P release from poultry litter biochar. Similarly, struvite-K was previously identified in various biochars.[17,52] However, the presence or absence of struvite or struvite-K in MgPA-BC could neither be confirmed nor be ruled out. Possibly, some of these phases may have been present in MgPA-BC, but were masked by other peaks in the XRD pattern and FTIR spectrum. The largely amorphous nature of MgPA-BC and the presence of SiO$_2$ made it difficult to confirm the specific orthophosphates.

Based on the identified phases in XRD and FTIR analysis, the phosphate release from MgPA-BC could be separated into two processes, namely: (1) dissolution of crystalline Mg$_2$P$_2$O$_7$, and (2) dissolution of an amorphous orthophosphate (such as struvite, struvite-K, and/or Mg$_3$(PO$_4$)$_2$). In the XRD pattern of MgPA-BC, α-Mg$_2$P$_2$O$_7$ was the sole crystalline phosphate phase,

and the intensity decreased during the dissolution process that suggested its dissolution. We could not find any reliable $K_{sp}$ values for $Mg_2P_2O_7$, but it can be inferred that $Mg_2P_2O_7$ is more soluble than $Ca_2P_2O_7$ since the presence of $Mg^{2+}$ ions was reported to increase the $Ca_2P_2O_7$ solubility.[34,53] The dissolution of $Mg_2P_2O_7$ likely took place *via* the release of pyrophosphate $(P_2O_7^{4-})$ ions, which likely remained in solution as pyrophosphate ions, since the conversion of pyrophosphate to orthophosphate takes place only very slowly at room temperature and neutral pH.[34] To confirm the release of condensed phosphates (such as pyrophosphates but also longer chains) from MgPA-BC, the solution after the 240 hour kinetic release experiment was digested with a persulfate solution (Table S3 in ESI†). After persulfate digestion, the dissolved P concentration after 240 hours was $68.4 \pm 3.3$ mg $L^{-1}$, which is higher than the P concentration before persulfate digestion ($49.6 \pm 1.4$ mg $L^{-1}$), indicating that indeed some $Mg_2P_2O_7$ dissolved. It should be noted that the P dissolution from $Mg_2P_2O_7$ cannot explain the phosphate release kinetics because the dissolved P concentrations in Fig. 3a consist primarily of orthophosphates.[54]
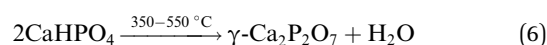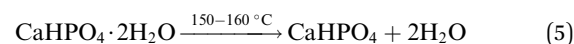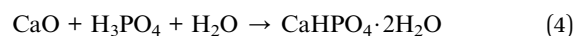
Thus, in addition to $Mg_2P_2O_7$ (the only crystalline phosphate phase), an (amorphous) orthophosphate also dissolved from MgPA-BC. To identify the determining phase for phosphate dissolution, the dissolved P concentrations from MgPA-BC were compared with calculated solubility values of various common Mg phosphates (Fig. 6). After 240 hours, struvite and $Mg_3(PO_4)_2 \cdot 22H_2O$ appear to be the rate-limiting phases for long-term phosphate dissolution; the dissolved P concentration agreed very well with the calculated solubility of struvite and $Mg_3(PO_4)_2 \cdot 22H_2O$ (see Fig. 6). Indeed, struvite/struvite-K and $Mg_3(PO_4) \cdot 22H_2O$ were the phases that appeared in the XRD pattern of MgPA-BC-post (Fig. 4). In previous experiments, struvite was in equilibrium with $Mg_3(PO_4)_2 \cdot 22H_2O$ under similar alkaline conditions.[55] The dissolved Mg concentration



Fig. 6 Comparison of the dissolved P concentrations of MgPA-BC with calculated solubility curves of various reference compounds. The arrow indicates the direction of change of the dissolved P concentrations throughout the 240 hour kinetic release experiment.

after 240 hours ($34.3 \pm 1.5$ mg $L^{-1}$) was similar to the dissolved P concentrations (Table S3 in ESI†), which further confirmed that an Mg-containing phosphate dissolved from the biochar.

Amorphous $Mg_3(PO_4)_2$ was possibly also present in MgPA-BC as suggested by the FTIR spectrum (Fig. 5) and previous work.[51] It is likely that the amorphous $Mg_3(PO_4)_2$ converted to crystalline $Mg_3(PO_4)_2 \cdot 22H_2O$ during the kinetic release experiment.

### 3.8 Formation and dissolution mechanism of CaPA-BC

Similar to MgPA-BC, the XRD pattern of CaPA-BC (Fig. 4) demonstrated the presence of crystalline $\gamma$-$Ca_2P_2O_7$ as the sole crystalline phosphate phase. The characteristic peaks of $\gamma$-$Ca_2P_2O_7$ were also prominent in the FTIR spectrum of CaPA-BC (Fig. 5), as well as the presence of needle-like or tabular crystals in the SEM image (Fig. 1c). In previous studies, crystalline $Ca_2P_2O_7$ was formed under similar pyrolysis conditions.[17,21,33] The formation pathway can be proposed as follows:

$$CaO + H_3PO_4 + H_2O \rightarrow CaHPO_4 \cdot 2H_2O \tag{4}$$

$$CaHPO_4 \cdot 2H_2O \xrightarrow{150-160\,°C} CaHPO_4 + 2H_2O \tag{5}$$

$$2CaHPO_4 \xrightarrow{350-550\,°C} \gamma\text{-}Ca_2P_2O_7 + H_2O \tag{6}$$

The reaction of CaO with $H_3PO_4$ resulted in the formation of $CaHPO_4 \cdot 2H_2O$.[23] Upon heating, the $CaHPO_4 \cdot 2H_2O$ was dehydrated to form $CaHPO_4$ at around 150–160 °C, which further converted into crystalline $\gamma$-$Ca_2P_2O_7$ at around 350–550 °C.[50,56]

Apart from $Ca_2P_2O_7$, other Ca phases may have been present as well, either as amorphous or small amounts of crystalline phases. Examples of phases that were previously observed in biochars prepared under similar conditions were $CaHPO_4$,[11,17,36] $Ca_3(PO_4)_2$, $Ca_8H_2(PO_4)_6 \cdot 5H_2O$,[22] and hydroxyapatite $(Ca_{10}(OH)_2(PO_4)_6)$.[17,22] When comparing the solubility of these phases with the dissolved P concentrations from CaPA-BC (Fig. 7), it appears that $\beta$-$Ca_3(PO_4)_2$ (*i.e.*, $(Ca,Mg)_3(PO_4)_2$) was the rate controlling phase, in agreement with the XRD pattern of CaPA-BC-post (Fig. 4). In addition, a more soluble phase such as (amorphous) $CaHPO_4$ was likely also present in CaPA-BC, as was suggested by the $HPO_4$ peak at 884 $cm^{-1}$ in the FTIR spectrum of CaPA-BC (Fig. 5) and since this phase was identified in various Ca- and P-rich biochars.[11,17,36]

Based on the identified phases, the phosphate dissolution from CaPA-BC was separated into two processes, namely (1) dissolution of crystalline $Ca_2P_2O_7$, and (2) dissolution of an amorphous orthophosphate (such as $(Ca,Mg)_3(PO_4)_2$ and/or $CaHPO_4$). The solubility of $Ca_2P_2O_7$ is very low, with reported $K_{sp}$ values ranging from $3 \times 10^{-18}$ to $1.8 \times 10^{-13}$.[53,57] Little to no dissolution of $Ca_2P_2O_7$ was also confirmed by the fact that the dissolved P concentrations before and after persulfate digestion were not different (Table S3 in ESI†). Lustosa Filho *et al.*[17] also found that crystalline $Ca_2P_2O_7$ was still present after their 240 hour kinetic release experiment of poultry litter biochars.

Similar to MgPA-BC, the phosphate dissolution from CaPA-BC cannot be solely ascribed to the formation of $Ca_2P_2O_7$, and an orthophosphate phase must have been responsible for the P
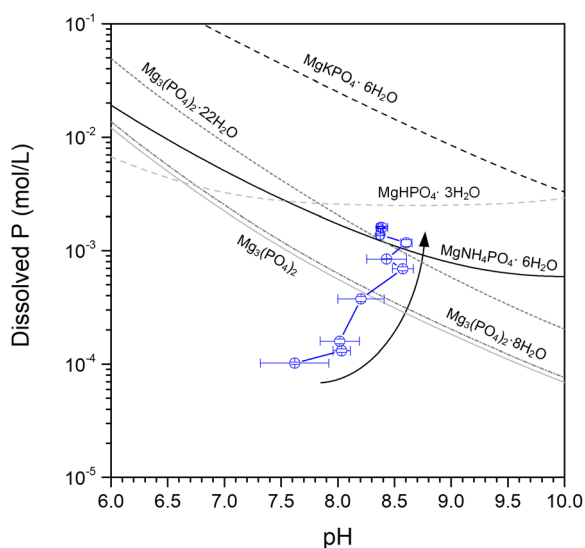
**Fig. 7** Comparison of the dissolved P concentrations of CaPA-BC with calculated solubility curves of various reference compounds. The arrow indicates the direction of change of the dissolved P concentrations throughout the 240 hour kinetic release experiment.
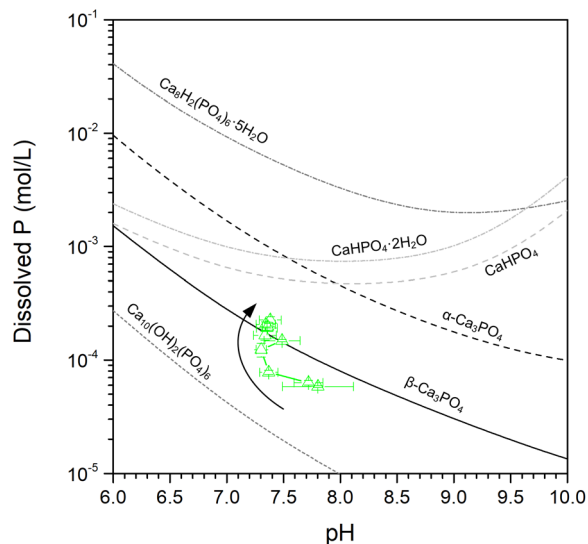
release. The dissolved P concentrations did not change any further after 144 hours (Fig. 3a) and equilibrium was reached. When comparing the dissolved P concentrations with the calculated solubilities of various Ca phosphates, the equilibrium P concentration was in good agreement with the calculated solubility of $\beta$-Ca$_3$(PO$_4$)$_2$ (Fig. 6b). This was further corroborated by the presence of (Ca,Mg)$_3$(PO$_4$)$_2$ in the XRD pattern of CaPA-BC-post (Fig. 4). In previous studies, the slow phosphate release and poor solubility of P and Ca from various biochars was also ascribed to crystalline (Ca,Mg)$_3$(PO$_4$)$_2$.[22,58] It should be noted that the actual solubility of (Ca,Mg)$_3$(PO$_4$)$_2$ may be lower than that of the calculated Mg-free $\beta$-Ca$_3$(PO$_4$)$_2$, depending on the Mg content.[46]

After 240 hours, close to 2% of the P present in CaPA-BC dissolved, and only 0.5% of the total Ca has dissolved (Table S3 in ESI†). This very low amount of Ca dissolved suggested that an additional phase different than CaHPO$_4$ or (Ca,Mg)$_3$(PO$_4$)$_2$ may have been responsible for P dissolution and/or the Ca may have reprecipitated on the biochar surface in the form of (Ca,Mg)$_3$(PO$_4$)$_2$.

## 4. Conclusions

In this study, sugarcane filter cake was pyrolyzed after pre-treatment with H$_3$PO$_4$ in the presence of MgO (MgPA-BC) or CaO (CaPA-BC) and the potential P availability of the biochars to crops was studied by extraction (DI water and 2% formic acid) and kinetic release in DI water. When prepared under identical conditions, co-pyrolysis of biomass with MgO and CaO produced biochars with identical P loadings of 73–74 g kg$^{-1}$ but with distinctly different P release profiles. The phosphate dissolution from MgPA-BC was gradual and reached 10 g P per kg biochar after 240 hours, and the rate-determining phases

were identified to be Mg pyrophosphate (Mg$_2$P$_2$O$_7$), struvite (MgNH$_4$PO$_4$·6H$_2$O), and cattiite (Mg$_3$(PO$_4$)$_2$·22H$_2$O). In contrast, CaPA-BC only released 1.2 g P per kg biochar and equilibrium was reached after 144 hours. Further P dissolution from CaPA-BC was limited by the low solubility of Ca pyrophosphate (Ca$_2$P$_2$O$_7$) and whitlockite ((Ca,Mg)$_3$(PO$_4$)$_2$). These results demonstrate that while both Mg and Ca aid to immobilize P in biochars, co-pyrolysis with MgO retains the P in a more soluble and available form than CaO. Therefore, for slow release fertilizer applications, addition of MgO (and not CaO) is recommended during co-pyrolysis. The phytoavailability of the biochar-based fertilizers should be confirmed in a plant study, which will be carried out in our future work.

## Author contributions

Kaewta Jetsrisuparb: conceptualization, methodology, resources, writing – review & editing, supervision, project administration, funding acquisition. Thanawan Jeejaila: investigation. Chanon Saengthip: investigation. Pornnapa Kasemsiri: writing – review & editing, supervision. Yuvarat Ngernyen: writing & editing, funding acquisition. Prinya Chindaprasirt: writing – review & editing. Jesper T. N. Knijnenburg: conceptualization, methodology, validation, formal analysis, investigation, writing – original draft, visualization, funding acquisition.

## Conflicts of interest

There are no conflicts to declare.

## Acknowledgements

## References

1 M. R. Hart, B. F. Quin and M. L. Nguyen, *J. Environ. Qual.*, 2004, **33**, 1954–1972.

2 J. J. Weeks and G. M. Hettiarachchi, *J. Environ. Qual.*, 2019, **48**, 1300–1313.

3 W. Pornprakun, S. Sungnul, C. Kiataramkul and E. J. Moore, *Adv. Differ. Equations*, 2019, **2019**, 257.

4 R. D. M. Prado, G. Caione and C. N. S. Campos, *Appl. Environ. Soil Sci.*, 2013, **2013**, 581984.

5 P. A. O. George, J. J. C. Eras, A. S. Gutierrez, L. Hens and C. Vandecasteele, *Waste Biomass Valorization*, 2010, **1**, 407–413.

6 J. Zheng, J. Han, Z. Liu, W. Xia, X. Zhang, L. Li, X. Liu, R. Bian, K. Cheng, J. Zheng and G. Pan, *Agric., Ecosyst. Environ.*, 2017, **241**, 70–78.

7 N. R. Pandit, J. Mulder, S. E. Hale, A. R. Zimmerman, B. H. Pandit and G. Cornelissen, *Sci. Total Environ.*, 2018, **637–638**, 1333–1341.

8 A. J. Eykelbosh, M. S. Johnson, E. Santos De Queiroz, H. J. Dalmagro and E. Guimarães Couto, *PLoS One*, 2014, **9**, e98523.

9 A. B. Speratti, M. S. Johnson, H. M. Sousa, G. N. Torres and E. G. Couto, *Agronomy*, 2017, **7**, 49.

10 T. K. Choudhary, K. S. Khan, Q. Hussain, M. Ahmad and M. Ashfaq, *Arabian J. Geosci.*, 2019, **12**, 617.

11 S. Bruun, S. L. Harmer, G. Bekiaris, W. Christel, L. Zuin, Y. Hu, L. S. Jensen and E. Lombi, *Chemosphere*, 2017, **169**, 377–386.

12 Y. Wang, Y. Lin, P. C. Chiu, P. T. Imhoff and M. Guo, *Sci. Total Environ.*, 2015, **512–513**, 454–463.

13 R. Li, W. Teng, Y. Li, W. Wang, R. Cui and T. Yang, *J. Cleaner Prod.*, 2017, **140**, 964–970.

14 C. Vogel and C. Adam, *Environ. Sci. Technol.*, 2011, **45**, 7445–7450.

15 M. Marcińczyk and P. Oleszczuk, *J. Cleaner Prod.*, 2022, **339**, 130685.

16 S. Suwanree, J. T. N. Knijnenburg, P. Kasemsiri, W. Kraithong, P. Chindaprasirt and K. Jetsrisuparb, *Biomass Bioenergy*, 2022, **156**, 106304.

17 J. F. Lustosa Filho, E. S. Penido, P. P. Castro, C. A. Silva and L. C. A. Melo, *ACS Sustainable Chem. Eng.*, 2017, **5**, 9043–9052.

18 X. An, Z. Wu, J. Yu, G. Cravotto, X. Liu, Q. Li and B. Yu, *ACS Sustainable Chem. Eng.*, 2020, **8**, 3181–3190.

19 Q. Liu, Z. Fang, Y. Liu, Y. Liu, Y. Xu, X. Ruan, X. Zhang and W. Cao, *Waste Manage.*, 2019, **87**, 71–77.

20 L. Fang, F. Yan, J. Chen, X. Shen and Z. Zhang, *ACS Sustainable Chem. Eng.*, 2020, **8**, 6611–6621.

21 L. Zhao, X. Cao, W. Zheng, J. W. Scott, B. K. Sharma and X. Chen, *ACS Sustainable Chem. Eng.*, 2016, **4**, 1630–1636.

22 K. Sun, M. Qiu, L. Han, J. Jin, Z. Wang, Z. Pan and B. Xing, *Sci. Total Environ.*, 2018, **634**, 1300–1307.

23 K. L. Elmore and T. D. Farr, *Ind. Eng. Chem.*, 1940, **32**, 580–586.

24 A. Enders and J. Lehmann, *Commun. Soil Sci. Plant Anal.*, 2012, **43**, 1042–1052.

25 N. Abeysinghe, K. Jetsrisuparb, K. H. T. Karunarathna, E. P. S. Chandana, S. Suwanree, P. Kasemsiri, P. Chindaprasirt and J. T. N. Knijnenburg, *J. Met., Mater. Miner.*, 2022, **32**, 124–133.

26 T. Wang, M. Camps-Arbestain, M. Hedley and P. Bishop, *Plant Soil*, 2012, **357**, 173–187.

27 Y. Liang, X. Cao, L. Zhao, X. Xu and W. Harris, *J. Environ. Qual.*, 2014, **43**, 1504–1509.

28 X. L. Huang and J. Z. Zhang, *Talanta*, 2009, **78**, 1129–1135.

29 B. Müller, *Swiss Federal Institute for Environmental Science and Technology (EAWAG)*, Kastanienbaum, Switzerland, 2015.

30 S. Li, S. Harris, A. Anandhi and G. Chen, *J. Cleaner Prod.*, 2019, **215**, 890–902.

31 J. O. Fernandes, C. A. R. Bernardino, C. F. Mahler, R. E. Santelli, B. F. Braz, R. C. Borges, M. C. da Cunha Veloso, G. A. Romeiro and F. H. Cincotto, *Water, Air, Soil Pollut.*, 2021, **232**, 67.

32 A. B. Speratti, M. S. Johnson, H. M. Sousa, H. J. Dalmagro and E. G. Couto, *GCB Bioenergy*, 2018, **10**, 272–286.

33 R. Gao, Q. Wang, Y. Liu, J. Zhu, Y. Deng, Q. Fu and H. Hu, *Energy Fuels*, 2019, **33**, 413–419.

34 K. P. Pritzker, in *Calcium Phosphates in Biological and Industrial Systems*, Springer, 1998, pp. 277–301.

35 L. Leng, Q. Xiong, L. Yang, H. Li, Y. Zhou, W. Zhang, S. Jiang, H. Li and H. Huang, *Sci. Total Environ.*, 2021, **763**, 144204.

36 G. Bekiaris, C. Peltre, L. S. Jensen and S. Bruun, *Spectrochim. Acta, Part A*, 2016, **168**, 29–36.

37 W. Jastrzebski, M. Sitarz, M. Rokita and K. Bułat, *Spectrochim. Acta, Part A*, 2011, **79**, 722–727.

38 B. Udvardi, I. J. Kovács, P. Kónya, M. Földvári, J. Füri, F. Budai, G. Falus, T. Fancsik, C. Szabó, Z. Szalai and J. Mihály, *Sediment. Geol.*, 2014, **313**, 1–14.

39 H. Yang, R. Yan, H. Chen, D. H. Lee and C. Zheng, *Fuel*, 2007, **86**, 1781–1788.

40 B. C. Cornilsen and R. A. Condrate Sr, *J. Phys. Chem. Solids*, 1977, **38**, 1327–1332.

41 M. V. Ramlogan and A. A. Rouff, *J. Therm. Anal. Calorim.*, 2016, **123**, 145–152.

42 O. Kaygili, C. Tatar and F. Yakuphanoglu, *Ceram. Int.*, 2012, **38**, 5713–5722.

43 B. Lothenbach, B. Xu and F. Winnefeld, *Appl. Geochem.*, 2019, **111**, 104450.

44 B. Cornilsen and R. Condrate Sr, *J. Inorg. Nucl. Chem.*, 1979, **41**, 602–605.

45 Z. Zyman, M. Epple, A. Goncharenko, D. Rokhmistrov, O. Prymak and K. Loza, *J. Mater. Sci.: Mater. Med.*, 2017, **28**, 52.

46 X. Li, A. Ito, Y. Sogo, X. Wang and R. Z. LeGeros, *Acta Biomater.*, 2009, **5**, 508–517.

47 S. A. Walling and J. L. Provis, *Chem. Rev.*, 2016, **116**, 4170–4204.

48 N. Petranović, U. Mioč and D. Minić, *Thermochim. Acta*, 1987, **116**, 137–143.

49 M. A. Aramendía, V. Borau, C. Jiménez, J. M. Marinas and F. J. Romero, *J. Colloid Interface Sci.*, 1999, **217**, 288–298.

50 B. C. Sales, B. C. Chakoumakos, L. A. Boatner and J. O. Ramey, *J. Non-Cryst. Solids*, 1993, **159**, 121–139.

51 M. A. Aramendía, V. Borau, C. Jiménez, J. M. Marinas, F. J. Romero and J. R. Ruiz, *J. Colloid Interface Sci.*, 1998, **202**, 456–461.

52 N. Prakongkep, R. J. Gilkes and W. Wiriyakitnateekul, *J. Plant Nutr. Soil Sci.*, 2015, **178**, 732–740.

53 W. E. Brown and T. M. Gregory, *Arthritis Rheum.*, 1976, **19**, 446–462.

54 E. A. Nagul, I. D. McKelvie, P. Worsfold and S. D. Kolev, *Anal. Chim. Acta*, 2015, **890**, 60–82.

55 A. W. Taylor, A. W. Frazier and E. L. Gurney, *Trans. Faraday Soc.*, 1963, **59**, 1580–1584.

56 M. El Hazzat, A. El Hamidi, M. Halim and S. Arsalane, *Materialia*, 2021, **16**, 101055.

57 B. H. Wiers, *Inorg. Chem.*, 1971, **10**, 2581–2584.

58 L. Zhao, X. Cao, Q. Wang, F. Yang and S. Xu, *J. Environ. Qual.*, 2013, **42**, 545–552.